LBL-14334
Preprint

# Lawrence Berkeley Laboratory

UNIVERSITY OF CALIFORNIA

RECEIVED
LAWRENCE
BERKELEY LABORATORY

JUL 5 1983

LIBRARY AND
DOCUMENTS SECTION

## Materials & Molecular Research Division

Submitted to the Journal of the American Ceramic Society

# AN EXPERIMENTAL ASSESSMENT OF PORE BREAKAWAY DURING SINTERING

M. Sakarcan, C.H. Hsueh, and A.G. Evans

April 1983

TWO-WEEK LOAN COPY

This is a Library Circulating Copy which may be borrowed for two weeks. For a personal retention copy, call Tech. Info. Division, Ext. 6782.

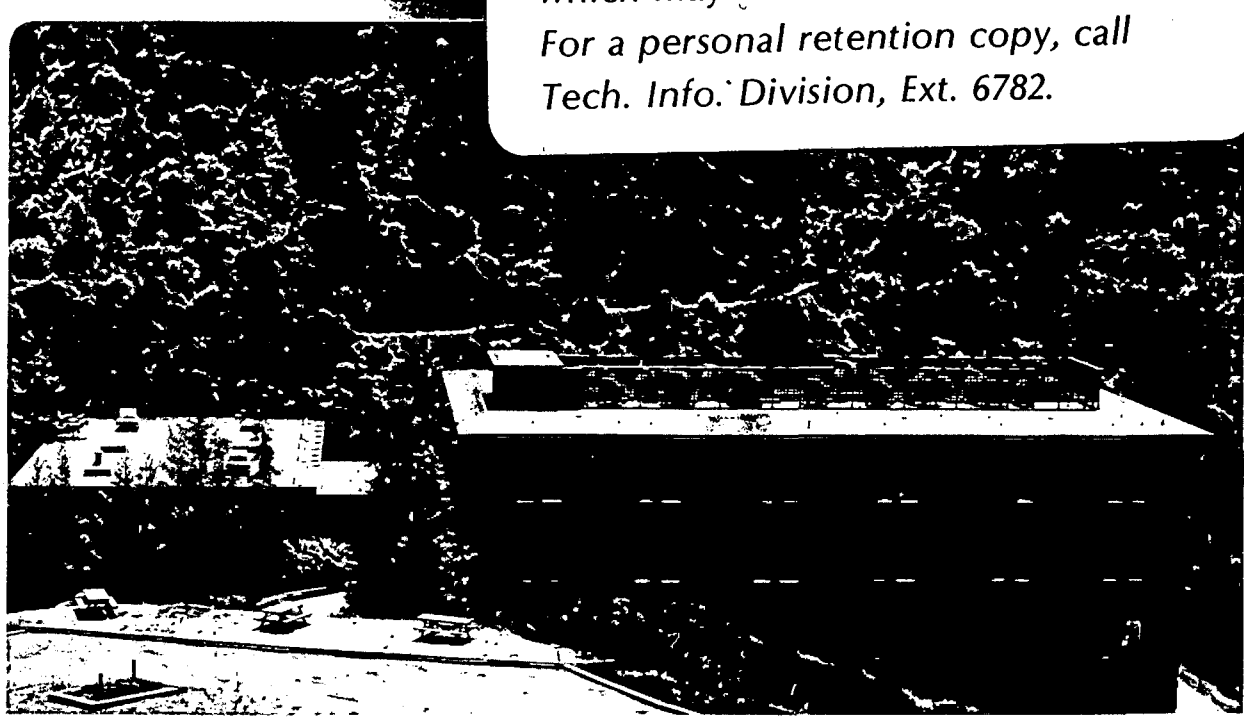

Prepared for the U.S. Department of Energy under Contract DE-AC03-76SF00098

LBL-14334 c.2

## DISCLAIMER

This document was prepared as an account of work sponsored by the United States Government. While this document is believed to contain correct information, neither the United States Government nor any agency thereof, nor the Regents of the University of California, nor any of their employees, makes any warranty, express or implied, or assumes any legal responsibility for the accuracy, completeness, or usefulness of any information, apparatus, product, or process disclosed, or represents that its use would not infringe privately owned rights. Reference herein to any specific commercial product, process, or service by its trade name, trademark, manufacturer, or otherwise, does not necessarily constitute or imply its endorsement, recommendation, or favoring by the United States Government or any agency thereof, or the Regents of the University of California. The views and opinions of authors expressed herein do not necessarily state or reflect those of the United States Government or any agency thereof or the Regents of the University of California.

# AN EXPERIMENTAL ASSESSMENT OF PORE BREAKAWAY DURING SINTERING

by

M. Sakarcan, C. H. Hsueh and A. G. Evans

Materials and Molecular Research Division, Lawrence Berkeley Laboratory
and Department of Materials Science and Mineral
Engineering, University of California
Berkeley, CA 94720

## ABSTRACT

Experimental measurements of intragranular pore size distributions and of the shapes of distorted pores attached to grain boundaries have been used to examine the pore/grain boundary separation problem. In-situ evaluation of the ratio of the boundary mobility to surface diffusivity from pore distortion measurements, coupled with prior analytic expressions for the critical pore breakaway condition, have permitted the prediction of specific intragranular pore sizes generated by separation. The predictions lie within the distribution of measured intragranular pore sizes.

This work was supported by the Director, Office of Energy Research, Office of Basic Energy Sciences, Materials Sciences Division of the U.S. Department of Energy under contract No. DE-AC03-76SF00098.

## 1. INTRODUCTION

Conditions pertinent to the separation of pores from grain boundaries during final stage sintering have been proposed in several recent analyses.[1-4] In particular, the analyses predict a lower bound, below which separation is prohibited at disappearing (three-sided) grains. This bound is dictated primarily by the grain boundary mobility, $M_b$, the dihedral angle, $\Psi$, and either the surface diffusivity, $D_s\delta_s$, or the vapor pressure, $p_o$. Specifically, when pore motion is surface diffusion dominated, separation is prohibited when the pore size, $a$, satisfies the inequality (fig. 1)[3];

$$a_c^2 \equiv 2\sqrt{3}(\Omega^{1/3}D_s\delta_s/M_b kT)(3-\Psi)\sec(\Psi/2) > a^2 \qquad (1a)$$

where $a_c$ is the critical pore size (above which separation of pores from grain boundaries may occur) and $\Omega$ is the atomic volume. Evaporation/condensation dominated pore motion dictates that separation is prohibited when,[4]

$$M_b < 2\sqrt{2/3\pi}\,[p_o m^{1/2}\Omega^{1/3}/\rho(kT)^{3/2}][0.13\Psi^2-0.85\Psi+1.4]\sec(\Psi/2) \qquad (1b)$$

where $m$ is the weight of a molecule and $\rho$ is the density of the material.

Separation above the lower bound is contingent upon the configuration of the associated grains (although the separation condition invariably becomes less stringent as the grain size increases). Specifically, for surface diffusion dominated pore motion, the separation of a pore from a grain boundary, with a radius of curvature $R$, is prohibited when,[3]

$$a^3/R < \sqrt{3}\,(\Omega^{1/3}D_s\delta_s/M_b kT)(3-\Psi)\sec(\Psi/2) \qquad (1c)$$

These concepts, and their implications, have yet to be subject to experimental validation. The intent of the present paper is to examine distributions of small, separated, intragranular pores in materials exhibiting final stage microstructures, in order to ascertain their consistency with the predictions of the separation model. This assessment is performed, using MgO, subject to pore size and temperature conditions which permit surface diffusion dominated pore motion.

The correlation between experiment and theory is contingent upon knowledge of the mobility ratio, $D_s\delta_s\Omega^{1/3}/M_b$ (eqn 1a), pertinent to the separation event. A method for in situ estimation of this ratio from the shapes of distorted pores attached to grain boundaries (which constitutes an important prerequisite to the analysis of separated pores) is described in the second section of the paper. Subsequent sections are concerned with the analysis of separated, intragranular pores and implications regarding the pertinence of the existing separation models to the formation of such pores.

## 2. EXPERIMENTAL

The material used for the present study was an undoped MgO purchased from Mallincrodt Chemical Company (refer to Table I for the chemical analysis). The original particle size ranged from 1 to 3 μm. The powder was calcined and vacuum hot pressed in a graphite die. The hot pressing temperatures (1200 to 1300°C) and pressures (18 to 35 MPa) were selected to achieve final stage microstructures. Following the hot pressing, the surfaces were mechanically removed and heat treated, in vacuo, at the

temperature ($\sim$ 1500°C) and time ($\sim$4h) needed to induce pore-grain boundary separation. Densities measured after hot pressing ($\sim 3.0 \times 10^3 \mathrm{Kg\,m^{-3}}$, $\sim$ 85% theoretical density) increased slightly after subsequent heat treatment (to $\sim 3.1 \times 10^3$ Kg $m^{-3}$). There was no overt evidence of local void volume increases (bloating) due to oxidation of carbon impurities. Subsequent fine polishing was conducted using diamond paste (6 μm) and $Al_2O_3$ powder (0.3 μm). The specimens were then thermally etched in air and examined using optical and scanning electron microscopy. Typical micrographs of separated intragranular pores and of distorted pores attached to grain boundaries are summarized in fig. 2.

## 3. THE MOBILITY RATIO

### 3.1 The Theoretical Basis

The axial shapes of distorted pores (fig. 3a) attached to grain boundaries are characterized by two dominant curvatures;[3]

$$\kappa_1^s = (d^2y/dx^2)[1 + (dy/dx)^2]^{-3/2}$$

$$\kappa_2^s = (1/x)(dy/dx)[1 + (dy/dx)^2]^{-1/2} \qquad (2)$$

where (x,y) are the coordinates of the pore surface. The curvature gradient dictates the atom flux, $j^s$, at each location on the pore surface in accord with the relation

$$j^s = -\left(\frac{D_s\delta_s\gamma_s}{kT}\right)[1 + (dy/dx)^2]^{-1/2}\left(\frac{d(\kappa_1^s + \kappa_2^s)}{dx}\right)$$

$$\equiv \lambda(x,y)\left(\frac{D_s\delta_s\gamma_s}{kT}\right) \qquad (3)$$

The velocity of the pore $v_p$ is then related to the flux gradient between adjacent surface positions $(x_1,y_1)$ and $(x_2,y_2)$ by;

$$v_p = 2\Omega \left[\frac{j_1^s x_1 - j_2^s x_2}{x_1^2 - x_2^2}\right] \equiv \left(\frac{\Omega D_s \delta_s \gamma_s}{kT}\right) (\Delta\lambda/\Delta x) \qquad (4)$$

The attached grain boundary (fig. 3b) also exhibits two dominant curvatures (again expressed in terms of the grain boundary profile by eqn 2) that dictate the axial grain boundary velocity (fig. 3b) in accord with the relation[3];

$$v_b = M_b \gamma_b \Omega^{2/3} (\kappa_1^b + \kappa_2^b)[1 + (dy/dx)^2]^{-1/2}$$

$$\equiv \zeta(x,y) M_b \gamma_b \Omega^{2/3} \qquad (5)$$

Recognizing that attachment requires equality of the pore and boundary velocity at the location $(x_o, 0)$ where the pore and boundary intersect (fig. 3a), eqns (4) and (5) yield the relation,

$$\frac{D_s \delta_s \Omega^{1/3}}{M_b kT} = 2\cos(\Psi/2) \left|\frac{\zeta}{\Delta\lambda/\Delta x}\right|_{(x_o,y_o)} \qquad (6)$$

Measurements of the pore and boundary shapes within the vicinity of the pore/boundary intersection (including measurements of $\Psi$) thus provide a basis for in-situ determination of the mobility ratio, $D_s \delta_s \Omega^{1/3}/M_b$ .

### 3.2 Measurements

Effective estimation of the mobility ratio from shape measurements on attached, distorted pores requires that the pore and boundary shape be determined with maximum precision. Consequently, since measurements could

only be performed on two dimensional sections, careful sectioning practice was required. The specific analyses were conducted by making shape measurements on sequential sections and identifying the section (e.g. fig. 2b) that afforded the closest representation of the desired axial configuration. The pore surface and grain boundary profiles at the axial configuration then yield direct estimates of the relative pore and boundary velocities for eqns (4) and (5): hence, permitting determination of the mobility ratio from the shape characteristics adjacent to the pore/boundary intersection (eqn 6). Studies of several pores, at different grain sizes, from sections that provide reasonable estimation of the axial configuration, reveal the pore curvature and flux and boundary velocity characteristics summarized in fig. 4. The resultant estimates of the mobility ratio, $D_s\delta_s\Omega^{1/3}/M_b$ , obtained from several distorted pores, exhibit values ranging between $10^{-33}Nm^3$ and $5 \times 10^{-33}Nm^3$ at 1500°C, with a discernable trend toward an increasing mobility ratio as the grain size increases.

A possible deficiency in the present estimate of the mobility ratio relates to its basis in the same mass transport relations used to predict the separation condition. Totally independent estimates of $M_b$ and $D_s\delta_s$ would perhaps be more convincing, provided that they could be obtained on the appropriate (small) scale, in material with a similar impurity content. However, the acquisition of pertinent data presents formidable experimental problems. In this context it is expedient to examine available data and to discuss their relevance to the present problem. Grain boundary mobility data obtained from grain growth measurements on a range of MgO materials[5] suggest a mobility for dense materials that ranges (at 1500°C) between $\sim 10^7 mN^{-1}s^{-1}$ for relatively pure material to $\sim 10^5 mN^{-1}s^{-1}$ for material

containing aliovalent $Fe^{3+}$ ions. The present material contains an appreciable concentration of aliovalent $Na^{+}$ ions (Table I). A mobility at the lower end of the range of the available data is thus probable. The surface diffusivity data, obtained from grain boundary grooving experiments on large MgO bicrystals[6-8], also indicate values that range over ∿2 orders of magnitude: specifically, at 1500°C, $D_s\delta_s$ varies between $\sim 3 \times 10^{-19}$ and $3 \times 10^{-21} m^3 s^{-1}$. Combining $D_s\delta_s$ with the most likely value of $M_b$, indicates a mobility ratio, $D_s\delta_s\ \Omega^{1/3}/M_b$, in the range $\sim 10^{-33}$ to $10^{-35} Nm^3$. The upper extreme approaches the value ascertained in the present study (from the pore/boundary shapes). This comparison suggests that the large extreme of the surface diffusivity values obtained on large bicrystals relates most closely to the motion of small pores. However, it is also evident that the wide range of $M_b$ and $D_s\delta_s$ values obtained from independent experiments prohibits accurate preselection of the mobility ratio pertinent to pores in a specific MgO compact.

## 4. INTRAGRANULAR PORE SIZE DISTRIBUTIONS

### 4.1 Measurements

The radii, r , of intragranular pores observed on polished sections have been measured on specimens subject to various annealing treatments. Histograms of the pore radii measured on samples annealed at 1500°C for 3, 6 and 12 h are presented in fig. 5. The corresponding grain sizes are listed in Table II.

The actual distribution of pore radii, a , can be deduced from the section radii, r , by applying the relation;[9]

$$f(a) = \frac{1}{\pi a} \int_{-\infty}^{a} (r^2 - a^2)^{1/2} f'(r)dr \qquad (7)$$

where $f(r)dr$ is the density distribution derived directly from the histograms of $r$ and $f(a)da$ is the density distribution of actual pore radii, $a$. The corresponding cumulative distribution is;

$$F(a) = \int_{-\infty}^{a} f(a)da \tag{8}$$

The cumulative pore size distributions deduced in this manner from the section size histograms are plotted in fig. 6. The median pore sizes for each distribution are listed in table II. Appreciable coarsening of the intragranular pores has evidently accompanied the grain growth. The extent of the coarsening is emphasized by the relative grain and pore size changes plotted in fig. 7.

## 4.2 The Coarsening Mechanism

The coarsening of intragranular pores can occur either by lattice diffusion between pores (in the presence of a pore size distribution), or by a sequence involving the reattachment of separated pores to a traversing boundary, subsequent coarsening by pore coalescence and eventual separation. The identification of the operative coarsening mechanism is a prerequisite for effective comparison between the theory of separation and the observed pore size distributions (as well as for the elucidation of grain size effects on separation). An upper bound estimate of the lattice diffusion contribution to pore coarsening can be obtained using the coarsening relation derived in the Appendix (eqn A6), by incorporating the effective lattice diffusivity;[10]

$$D_\ell = 2D_\ell^{Mg^{2+}} D_\ell^{O^{2-}} \Big/ \left[D_\ell^{Mg^{2+}} + D_\ell^{O^{2-}}\right] \tag{9}$$

Diffusivity measurements for MgO[11] suggest that (at 1500°C), $D_\ell^{Mg^{2+}} \approx 10^{-14} m^2 s^{-1}$, while $D_\ell^{O^{-2}} \approx 10^{-17} m^2 s^{-1}$: yielding a resultant diffusivity, $D_\ell = 2 \times 10^{-17} m^2 s^{-1}$. This choice for the diffusivity results in the coarsening plotted on fig. 7. The relatively smaller predicted coarsening rate suggests that the dominant coarsening occurs by processes other than lattice diffusion (involving the reattachment of pores to grain boundaries and subsequent pore coalescence).

A reattachment mode of coarsening implies the operation of several sequential events (occurring in conjunction with grain growth). Elucidation of the required coarsening sequence provides useful insights concerning the separation process and provides the basis for further analysis. Grain boundaries traverse specific location within a material several times during the grain growth process. Intragranular pores separated from grain boundaries during the early stages of grain growth can consequently reattach to a grain boundary that traverses the same region during subsequent grain growth. Reattachment is generally favored because the initially separated pores are likely to detach from disappearing (three-sided) grains subject to a monotonically increasing driving force (fig. 8a); whereas the traversing boundary (usually associated with a grain having > 5 sides) is subject to a lower, approximately uniform, driving force (fig. 8b). Additionally, initial separation occurs with some preference (fig. 1) for those boundaries that exhibit boundary energies at the extreme minimum of the $\gamma_b$ spectrum (e.g. coincidence site boundaries with dihedral angles $\rightarrow \pi$); whereas the traversing boundary is likely to exhibit a (more typical) larger $\gamma_b$, and hence, be more adherent. However, the <u>coarsening</u> of

reattached pores in microstructures of the type depicted in fig. 2 usually occurs[†] when the pores converge onto a grain corner and coalesce.[12] This process entails pore/grain boundary motion within a disappearing (three-sided) grain subject to a continuously increasing driving force (fig. 8a). The pores should thus separate before convergence, unless some of the parameters that dictate separation change during grain growth. The observed intragranular pore coarsening may thus be considered to imply an increase in the critical pore size $a_c$, with increase in grain size (that resides in the concomitant changes in the parameters that control $a_c$). Since the pores all exhibit radii $\lesssim 5$ μm, pore motion by evaporation/condensation can be excluded.[4] Hence, reference to eqn (1a) suggests a qualitative interpretation of the pore coarsening based on an increase in $D_s\delta_s$ or a decrease in $M_b$ with grain enlargement, or a change in the spectrum of dihedral angles toward a larger proportion of general (large $\gamma_b$) boundaries (at the expense of special boundaries).[††] A decrease in $M_b$ with grain growth is plausible by virtue of an increase in the grain boundary concentration of aliovalent solutes (e.g. $Na^+$) as the grain boundary area decreases during grain growth (thereby, enhancing the magnitude of the solute drag[5]). Specifically, the observed extent of pore coarsening (fig. 7) would suggest a decrease in grain boundary mobility by a factor of $\sim 5$, for a similar increase in the grain size. A trend of this type is apparent from the mobility ratio determinations

---

[†]Alternative coalescence processes may operate[13] in the presence of a continuous liquid phase.

[††]The dihedral angle effect is probably of secondary significance because $a_c$ varies by < 50% over the entire spectrum of $\Psi$ (fig. 1).

(section 3). Potential changes in $D_s\delta_s$ or $\Psi$ could also be conjectured, but the expected trends are ambiguous. Further coarsening studies are evidently needed to gain a more complete appreciation of this phenomenon, based upon changes in the mobility parameter during grain growth.

## 5. THE CRITICAL PORE SIZE

A critical pore size prediction may be deduced from fig. 1, by invoking the average mobility ratio evaluated in section 3 ($D_s\delta_s\Omega^{1/3}/M_b = 2 \times 10^{-23} Nm^3$) and adopting a typical dihedral angle of $2\pi/3$. This prediction yields, $a_c \approx 0.3$ μm, which lies within the low extreme of the measured pore radius distribution (fig. 7). Additionally, the condition pertinent to the separation of pores from grain boundaries having a radius of curvature equal to the average values at each grain size[5], $\langle R \rangle = \langle G \rangle/3$, may be evaluated from eqn (1c), as plotted on fig. 7. The pore sizes required for this mode of separation appear to be appreciably in excess of the measured intragranular pore sizes. Consequently, the present data and analysis suggest that the intragranular pores have, most probably, been generated by a mechanism involving the separation of pores from the boundaries of disappearing grains (the increase in separated pore size with increase in grain size being attributed to the corresponding decrease in grain boundary mobility assoicated with the grain boundary area decrease that accompanies grain growth).

Recognition of the uncertainties associated with the magnitude of the mobility parameter, and its grain size dependence, requires that the preceding conclusions be regarded as tentative, until more comprehensive mobility data are generated. The acquisition of the pertinent mobility data constitutes a formidable experimental problem, but is of paramount importance to the quantitative interpretation of pore separation measurements based on intragranular pore size distributions.

## 6. CONCLUSIONS

Measurements of the ratio of the grain boundary mobility to the surface diffusivity in MgO (obtained from the distortion of pores attached to grain boundaries) have been used, in conjunction with prior analytic expressions for pore breakaway, to predict the specific sizes of intragranular pores. The predictions lie within the measured intragranular pore size distributions. Preliminary credence in the present comprehension of the pore breakaway phenomenon is thereby established.

An observed trend toward increasing intragranular pore sizes with increase in grain size has yet to be fully explained. Intragranular pore coarsening by lattice diffusion has been excluded, based upon the available $Mg^{2+}$ and $O^{2-}$ diffusivity data. The coarsening would thus appear to be related to pore reattachment by traversing grain boundaries (during grain growth) and subseqent pore coalescence at disappearing grains. However, this interpretation is only tenable if the separation of pores from disappearing (three-sided) grains becomes more difficult as the grains enlarge or, alternatively, if pore separation from disappearing grains is rendered less critical than pore separation from the boundaries of average sized (> 5 sided) grains. The latter interpretation has been considered unlikely because the pore sizes for separation from grain boundaries with the average curvature, at each grain size, appreciably exceed the measured intragranular pore sizes (at least, within the uncertainties associated with the present estimate of the mobility ratio). The most plausible interpretation of the observed coarsening is

attributed to a decrease in grain boundary mobility during grain enlargement, associated with the decrease in grain boundary area that accompanies grain growth (resulting in a suppression of the pore separation event at the boundaries of disappearing grains, as the grain size increases). Preliminary mobility measurements confirm the existence of the requisite mobility trend. However, more comprehensive mobility measurements are needed to further explore the precise origin of the coarsening phenomenon.

ACKNOWLEDGMENT

This work was supported by the Director, Office of Energy Research, Office of Basic Energy Sciences, Materials Science Division of the U.S. Department of Energy under Contract No. DE-AC03-76SF00098.

## APPENDIX

### Intragranular Pore Coarsening By Lattice Diffusion

The particle coarsening analysis proposed by Greenwood[14] can be readily extended to the problem of intragranular pore coarsening by lattice diffusion. The motion of atoms between adjacent pores is dictated by the chemical potential difference,

$$\Delta\mu = 2\gamma_s\Omega(1/a_1 - 1/a_2) \tag{A1}$$

where $a_1$ and $a_2$ are the radii of the adjacent pores. The chemical potential dictates the flux,

$$j_\ell = \frac{D_\ell}{\Omega kT}\left(\frac{\Delta\mu}{\ell}\right) \tag{A2}$$

where $D_\ell$ is the lattice diffusivity and $\ell$ is the interpore spacing. The volume rate of flow of atoms between pores, through the intervening diffusive cross section, A , is thus,

$$\dot{V} = \frac{2\gamma_s\Omega D_\ell}{kT}\left(\frac{A}{\ell}\right)\left(\frac{1}{a_1} - \frac{1}{a_2}\right) \tag{A3}$$

But, matter conservation requires that,

$$\dot{V} = 4\pi a^2\dot{a} \tag{A4}$$

Hence, the growth rate of the larger pore, $\dot{a}_2$ , becomes;

$$2\, a_2^2\, \dot{a}_2 = \frac{\gamma_s\Omega D_\ell}{kT}\left(\frac{A}{\ell}\right)\left(\frac{1}{a_1} - \frac{1}{a_2}\right)$$

Following the same procedure adopted by Greenwood[14], the growth of the <u>fastest</u> growing pore $\hat{a}$ within a distribution of pores, can then be related

to the initial size of the pore, $\hat{a}_0$ , by;

$$\hat{a}^3 - \hat{a}_0^3 = 6D_\ell \Omega \gamma_s t/kT \tag{A6}$$

This relation provides an upper bound estimate of the pore coarsening by lattice diffusion.

## References


1. R. J. Brook, "Pore-Grain Boundary Interactions and Grain Growth," J. J. Am. Ceram. Soc., 52 [1] 56-57 (1969).
2. F. M. A. Carpay, "Discontinuous Grain Growth and Pore Drag," J. Am. Ceram. Soc., 60 [1] 82-83 (1977).
3. C. H. Hsueh, A. G. Evans and R. L. Coble, "Microstructure Development During Final Stage Sintering - I. Pore/Grain Boundary Separation," Acta Met., 30 [7] 1269-79 (1982).
4. C. H. Hsueh and A. G. Evans, Acta Met., in press.
5. M. F. Yan, R. M. Cannon and H. K. Bowen, Ceramic Microstructures (Ed. J. A. Pask and R. M. Fulrath), Westview (1976) p. 276.
6. J. Henney and J. W. S. Jones, "Surface-Diffusion Studies on $UO_2$ and MgO," J. Mater. Sci., 3 [2] 158-64 (1968).
7. W. M. Robertson, Sintering and Related Phenomenon (Ed. G. C. Kuczynski) Gordon & Breach, N.Y. (1967) p. 251.
8. S. A. Lytle and V. S. Stubican, "Surface Diffusion in MgO and Cr-Doped MgO," J. Am. Ceram. Soc., 65 [4] 210-12 (1982).
9. J. W. Cahn and R. L. Fullman, "On the Use of Linear Analysis for Obtaining Particle Size Distribution Functions in Opaque Samples," Trans AIME, 206, 610-13 (1956).
10. R. M. Cannon and R. L. Coble, Deformation of Ceramic Materials (Ed. R. C. Bradt and R. E. Tressler), Plenum, N.Y. (1974) p. 61.
11. W. D. Kingery, H. K. Bowen and D. Uhlmann, Introduction to Ceramics, Wiley, N.Y. (1978).
12. W. D. Kingery and B. Francois, Sintering and Related Phenomena, (Ed. G. C. Kuczynski), Gordon & Breach (1967) p. 471.

13. G. Rossi and J. E. Burke, "Influence of Additives on the Microstructure of Sintered $Al_2O_3$," J. Am. Ceram. Soc., 56 [12] 654-59 (1973).

14. G. W. Greenwood, "Growth of Dispersed Precipitates in Solutions," Acta Met., 4 [3] 243-48 (1956).

TABLE I

Chemical Analysis of the MgO Powder

| | |
|---|---|
| Barium (Ba) | 0.005% |
| Calcium (CaO | 0.05% |
| Chloride (Cl) | 0.01% |
| Iron (Fe) | 0.01% |
| Manganese (Mn) | 0.0005% |
| Nitrate ($NO_3$) | 0.005% |
| Potassium (K) | 0.005% |
| Sodium (Na) | 0.5% |
| Strontium (Sr) | 0.005% |

Table II

Intragranular Pore and Grain Size Variations

| Annealing Time (h) | Average Grain Diameter (μm) | Median Pore Radius (μm) |
|---|---|---|
| 0 | 8.8 | 0.32 |
| 3 | 15.6 | 0.53 |
| 6 | 25.6 | 0.60 |
| 12 | 35.0 | 0.78 |
| 24 | 48.0 | 0.95 |

## Figure Captions

Fig. 1. A plot of the critical pore size for pore/grain boundary separation when pore motion is dominated by surface diffusion.

Fig. 2. Scanning electron micrographs of pores
a) Separated intragranular pores
b) Distorted pores attached to grain boundaries.

Fig. 3a. A schematic of the distortion that accompanies the motion of pores attached to grain boundaries.

Fig. 3b. A schematic of the distortion of grain boundaries attached to moving pores.

Fig. 4. Characteristics of distorted pores and boundaries
a) the curvature variation across a pore surface, b) the atom flux along a pore surface and c) the velocity variation along an attached grain boundary.

Fig. 5. Histograms of the radii of the pores measured on polished sections.

Fig. 6. Cumulative distributions of actual pore radii determined from fig. 5.

Fig. 7. The variation in the median intragranular pore size with the average grain size. Also shown are: the relative pore coarsening attributed to lattice diffusion, the predicted critical pore size for pore/boundary separation, and the pore sizes required for the separation of pores from grain boundaries with the average radius of curvature at each grain size.

Fig. 8. Schematic illustrating the motion of pores attached to a) disappearing grains with a driving force that increases during disappearance, $R_{b_1} > R_{b_2}$ b) grains with a uniform driving force accompanying grain growth.

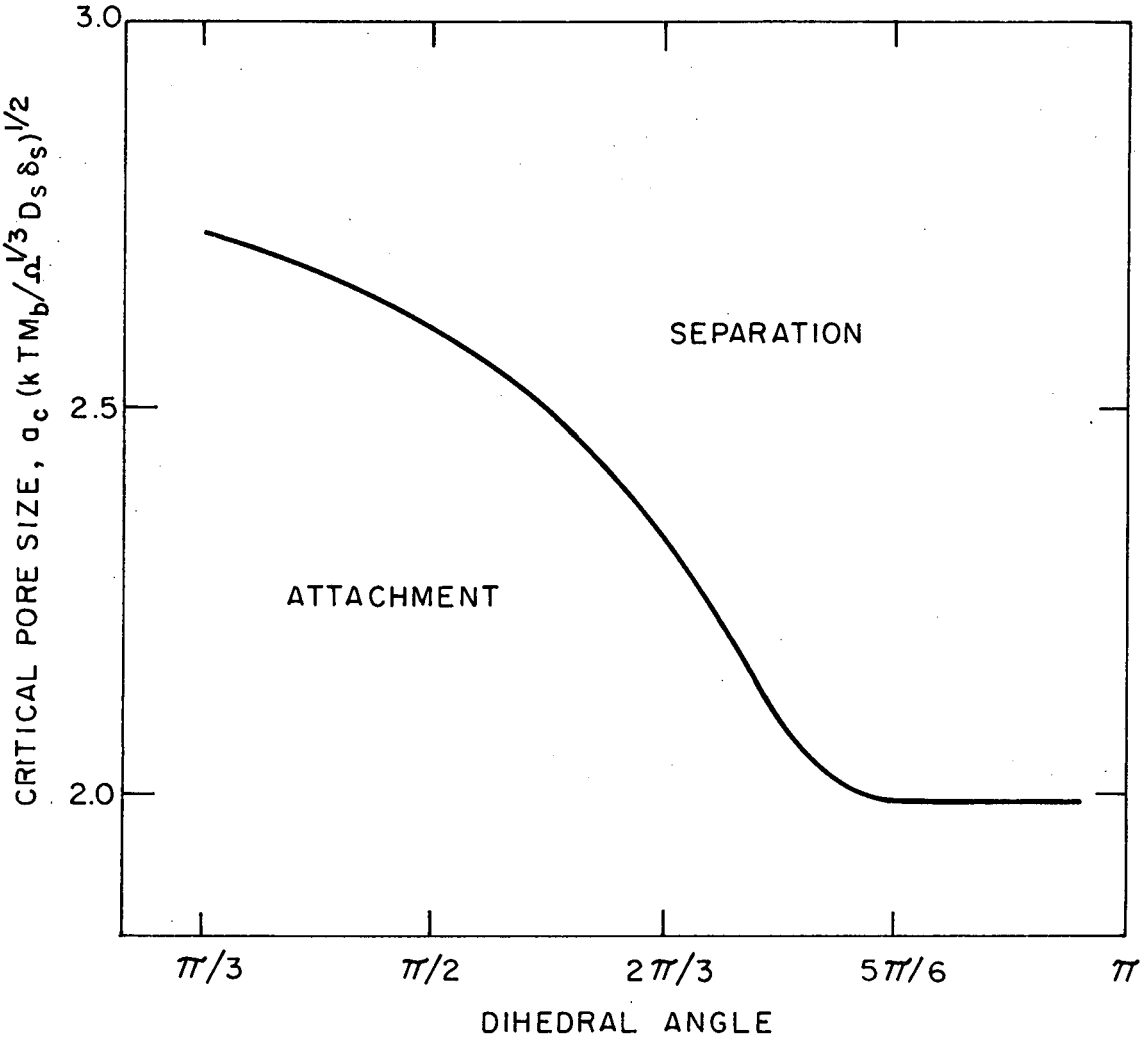


XBL 826-5899

Fig. 1

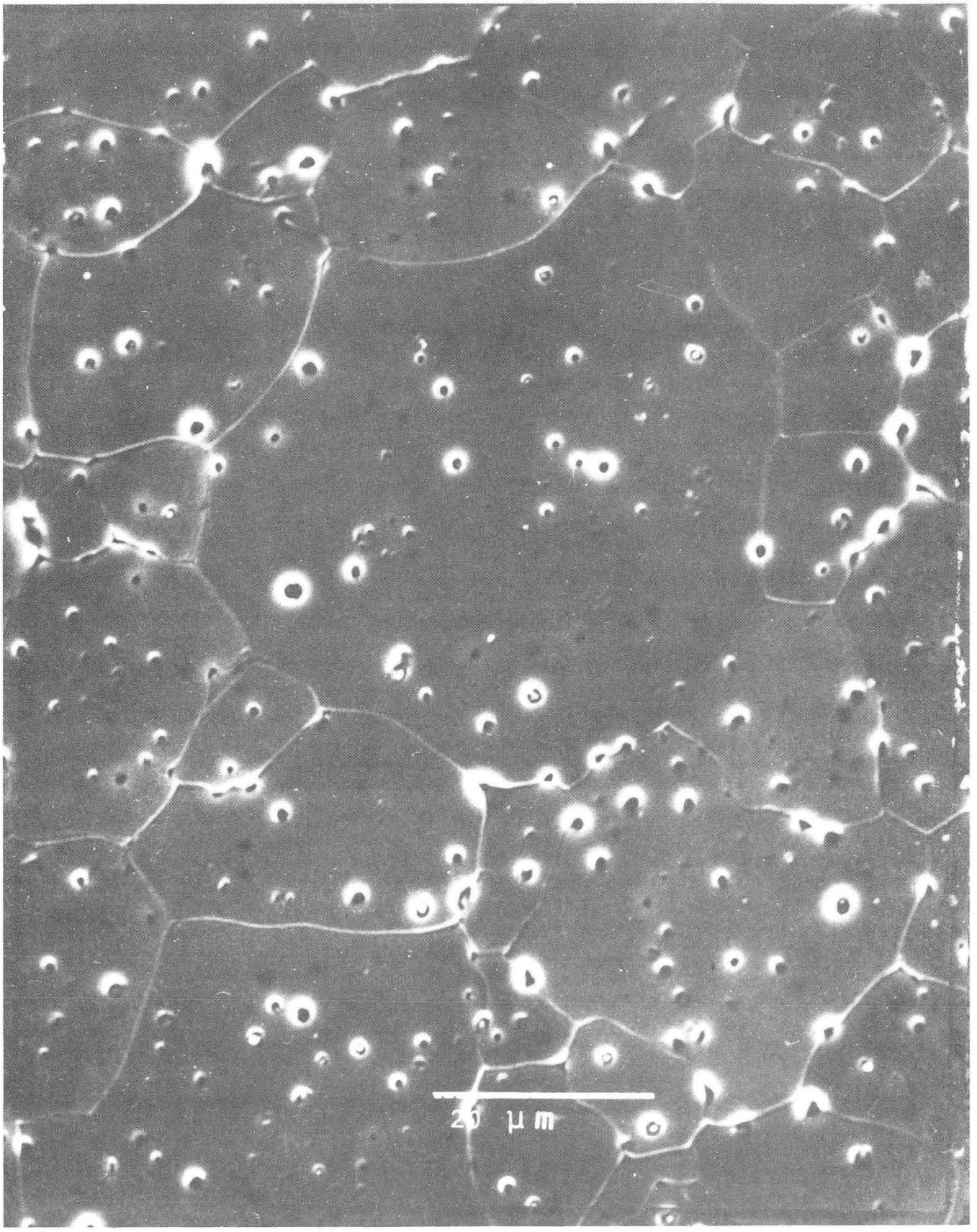


XBB815-4880

Fig. 2a

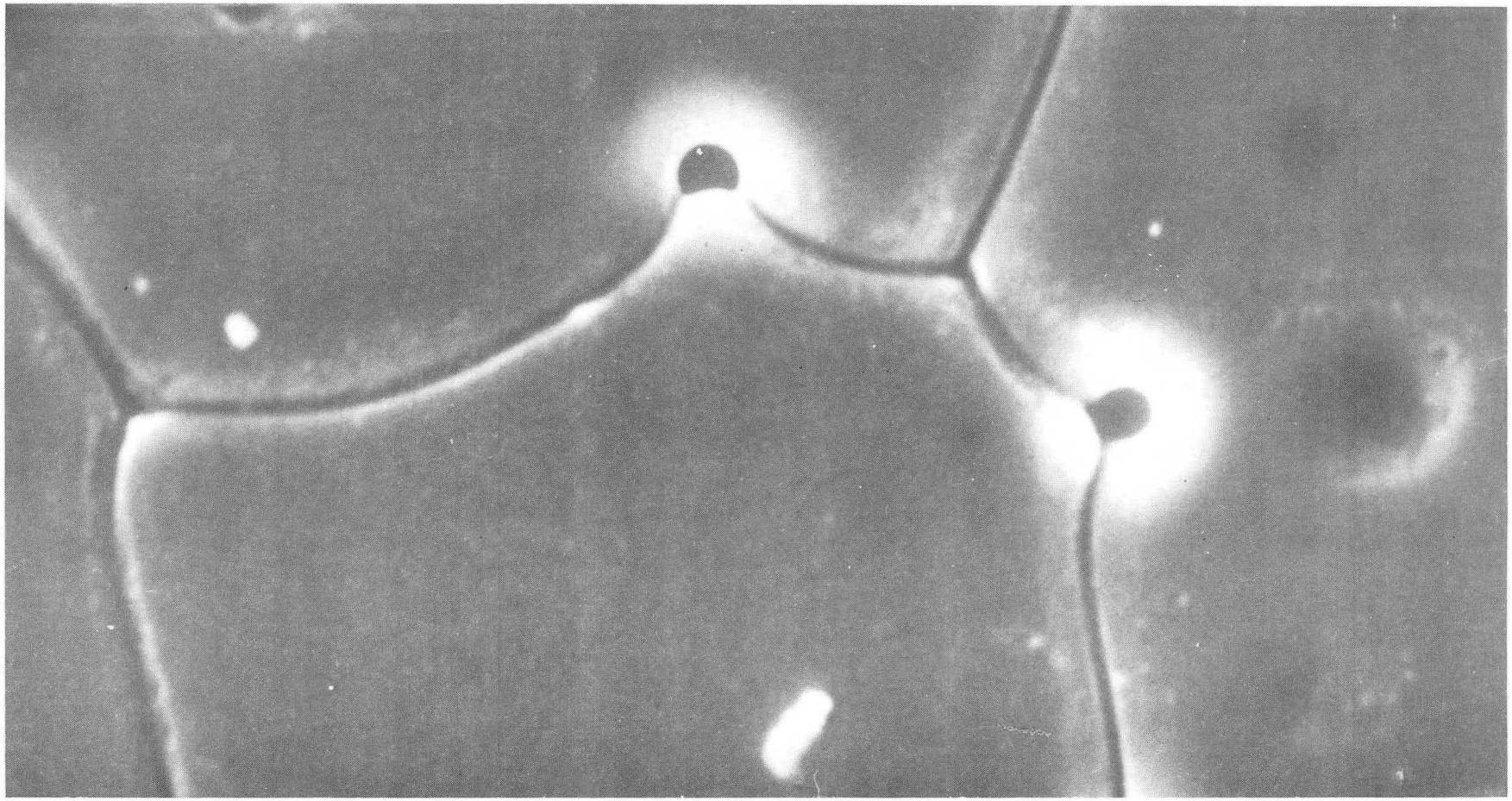

XBB810-9503

Fig. 2b

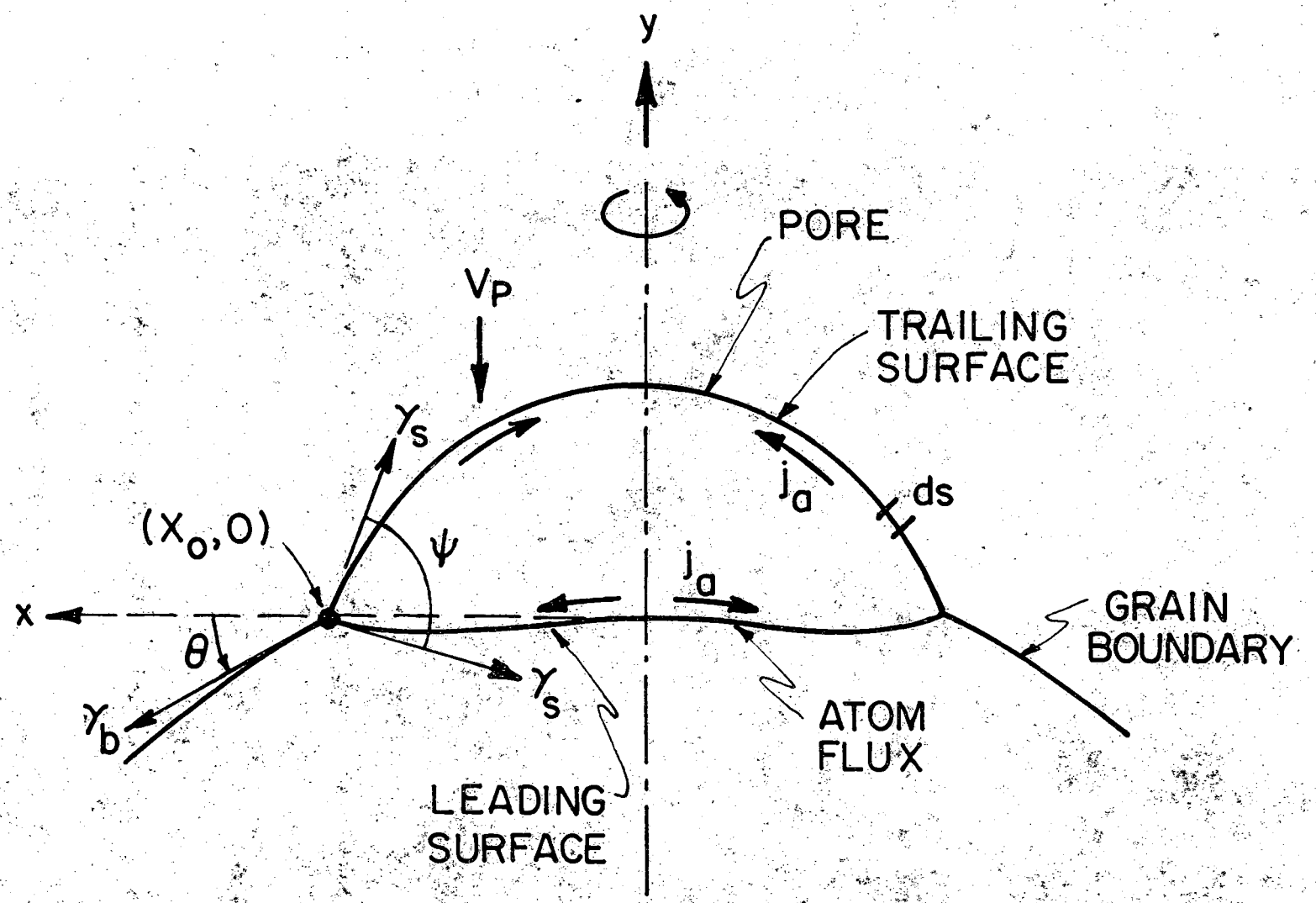


XBL 826-5907

Fig. 3a

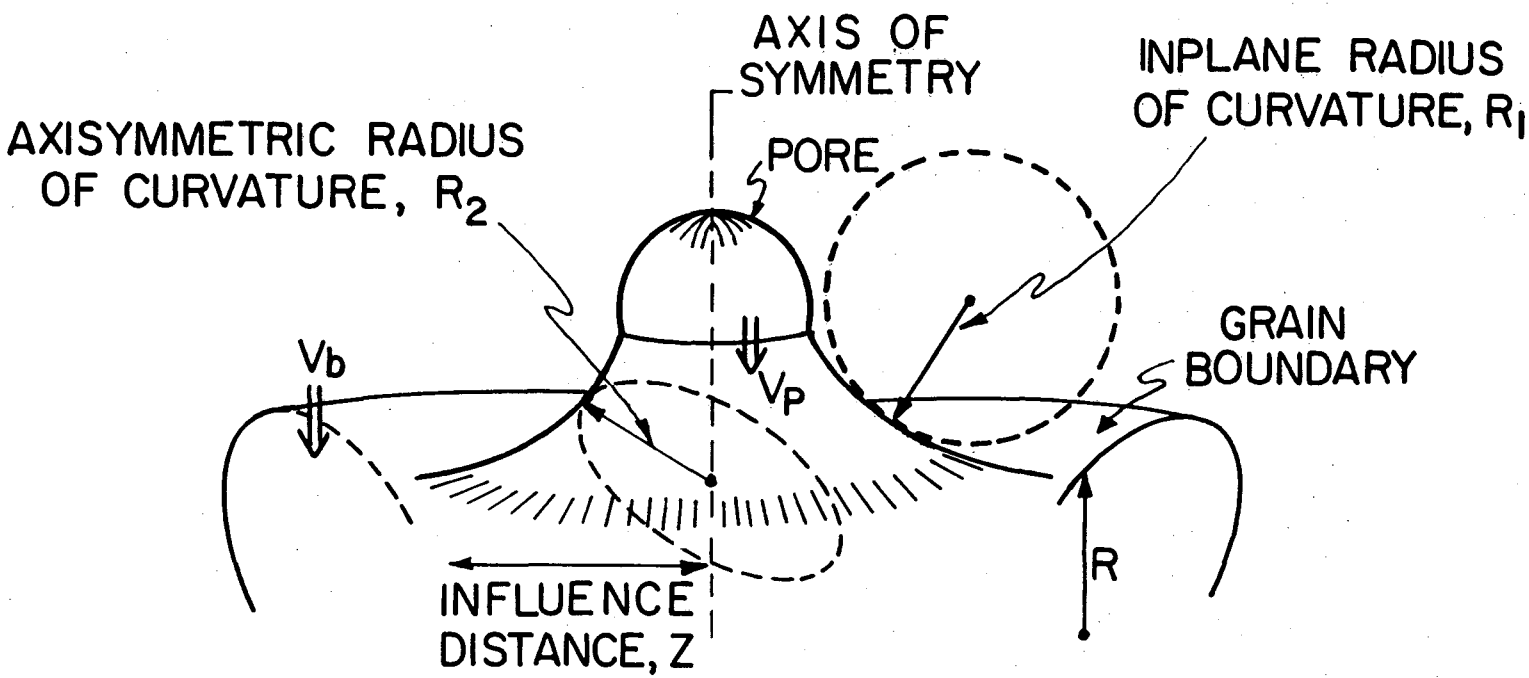


XBL 816-5979

Fig. 3b

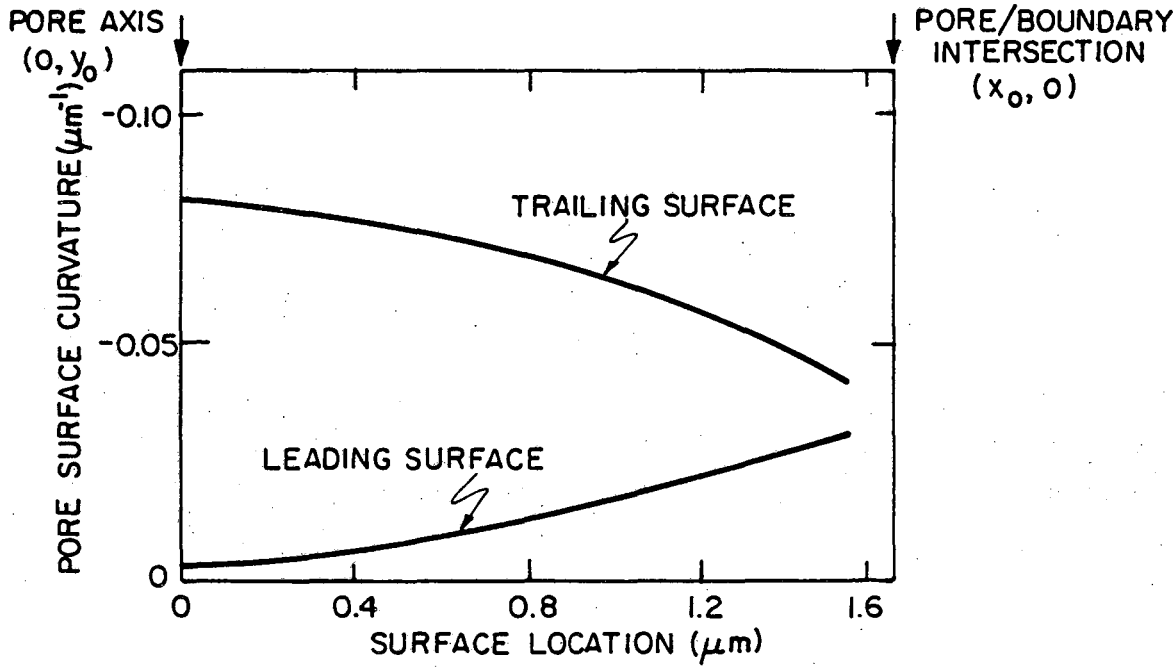


a) THE PORE SURFACE CURVATURES

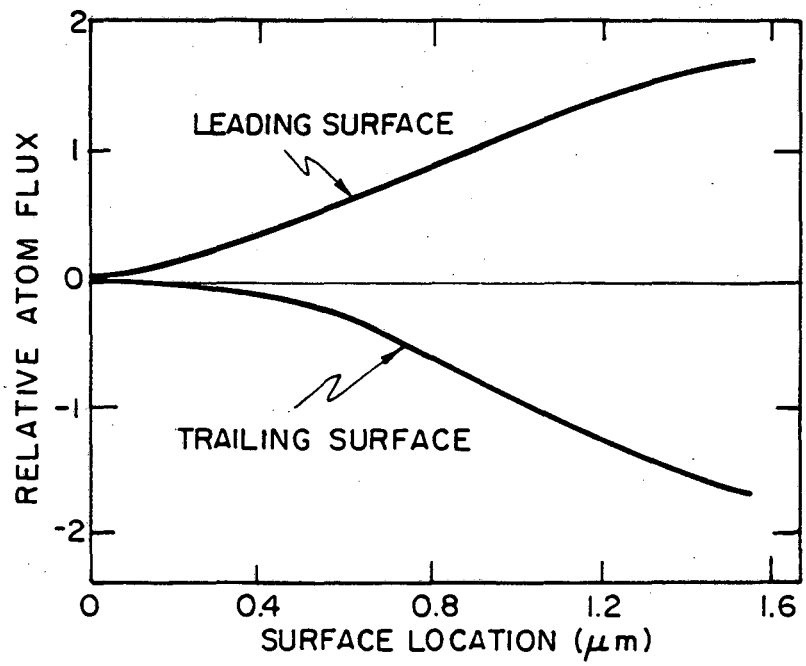


b) THE RELATIVE ATOM FLUXES ALONG THE PORE SURFACE

XBL826-5900

Fig. 4a,4b

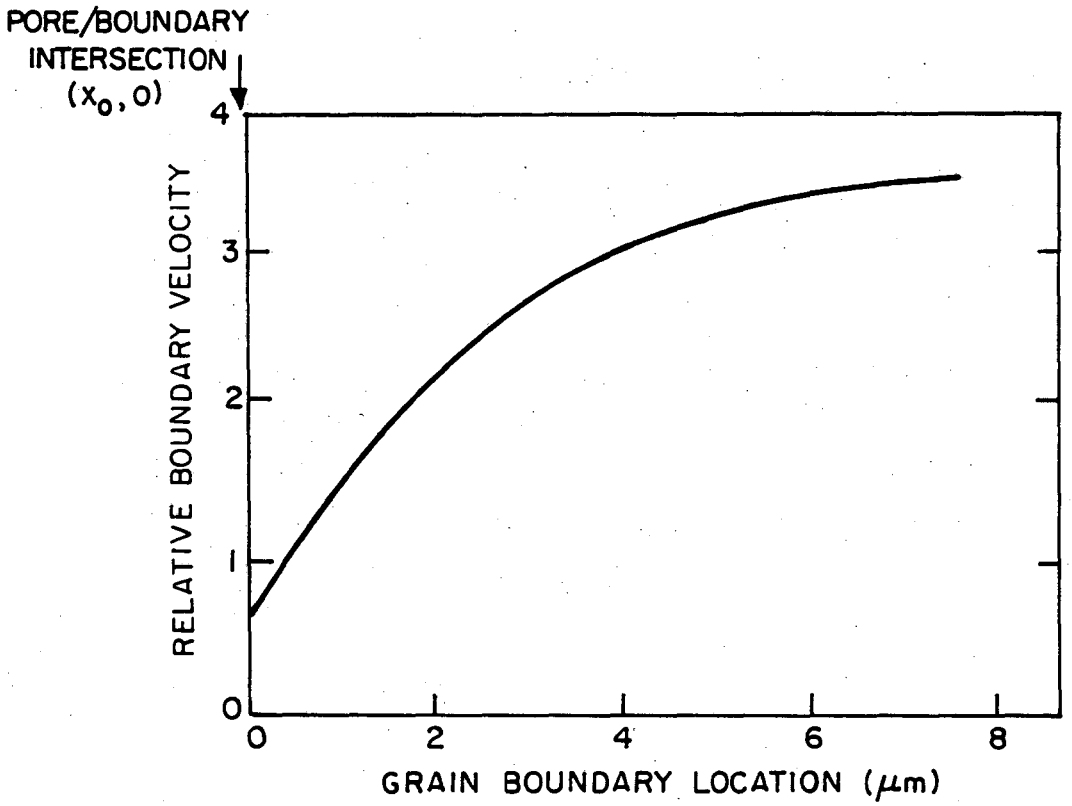


c) RELATIVE GRAIN BOUNDARY VELOCITY

XBL826-5901

Fig. 4c

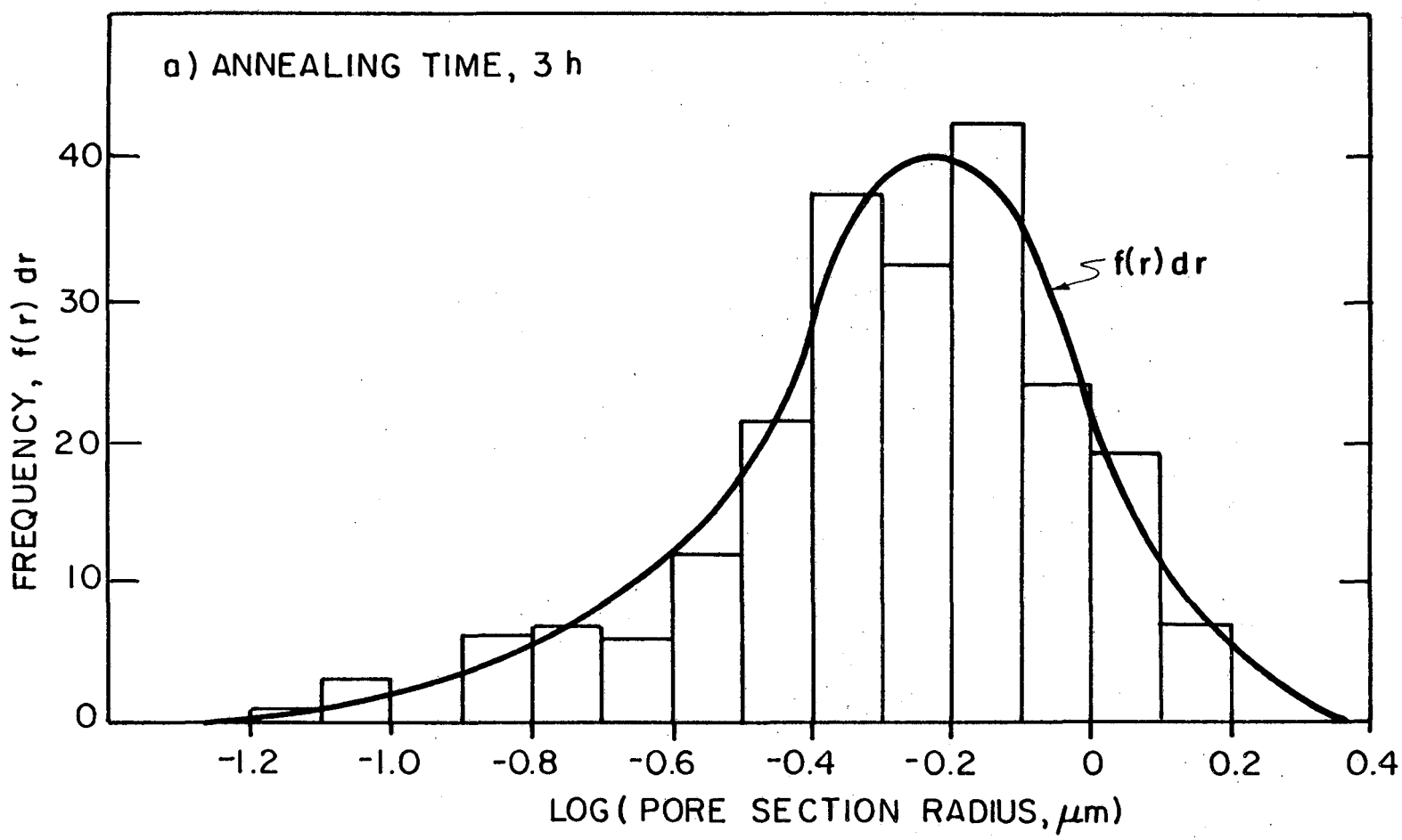


XBL 826-5902

Fig. 5a

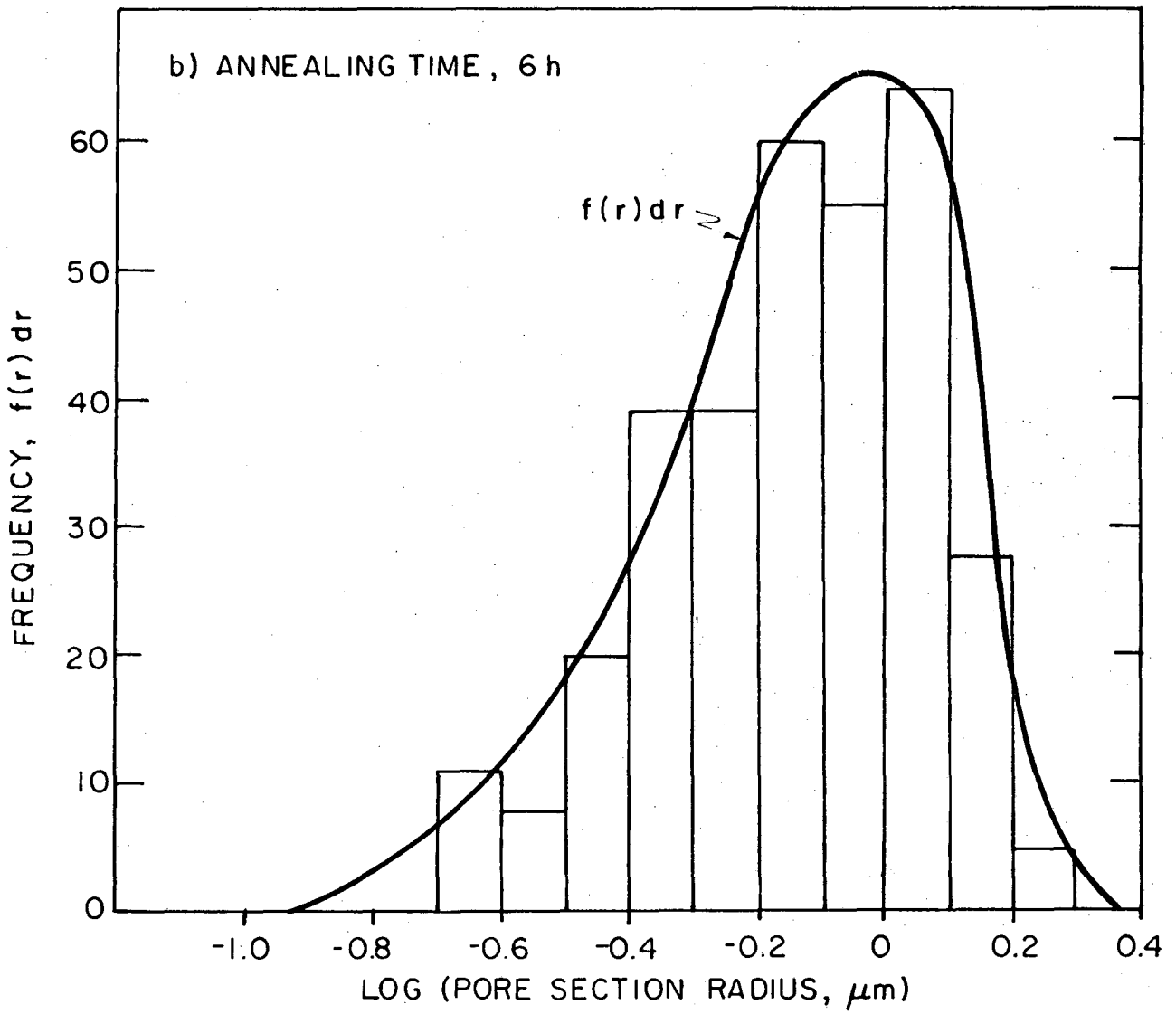


XBL 826-5903

Fig. 5b

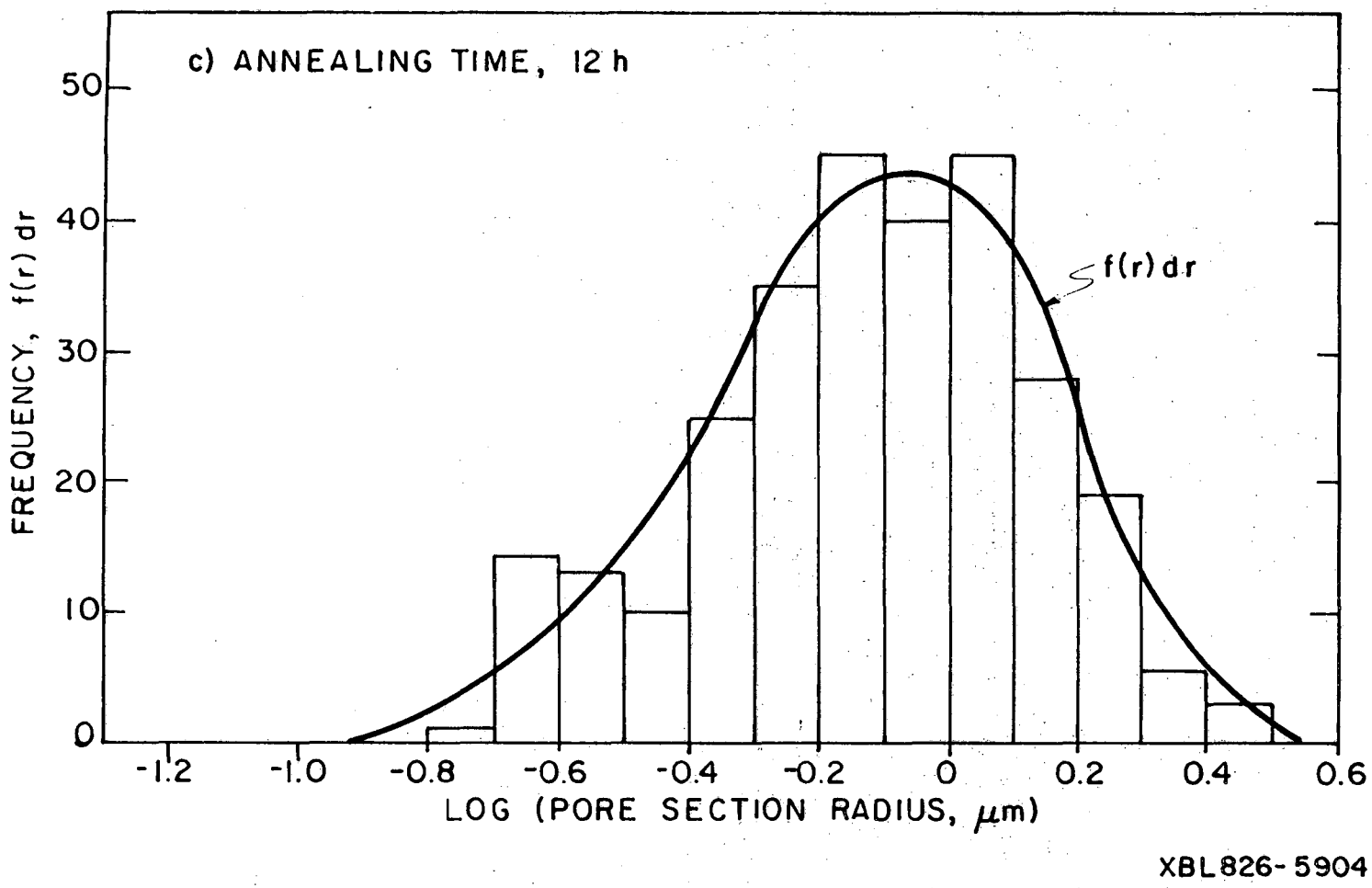
c) ANNEALING TIME, 12 h
FREQUENCY, f(r) dr
50
40
30
20
10
0
-1.2
-1.0
-0.8
-0.6
-0.4
-0.2
0
0.2
0.4
0.6
LOG (PORE SECTION RADIUS, μm)
f(r) dr
XBL826-5904

Fig. 5c

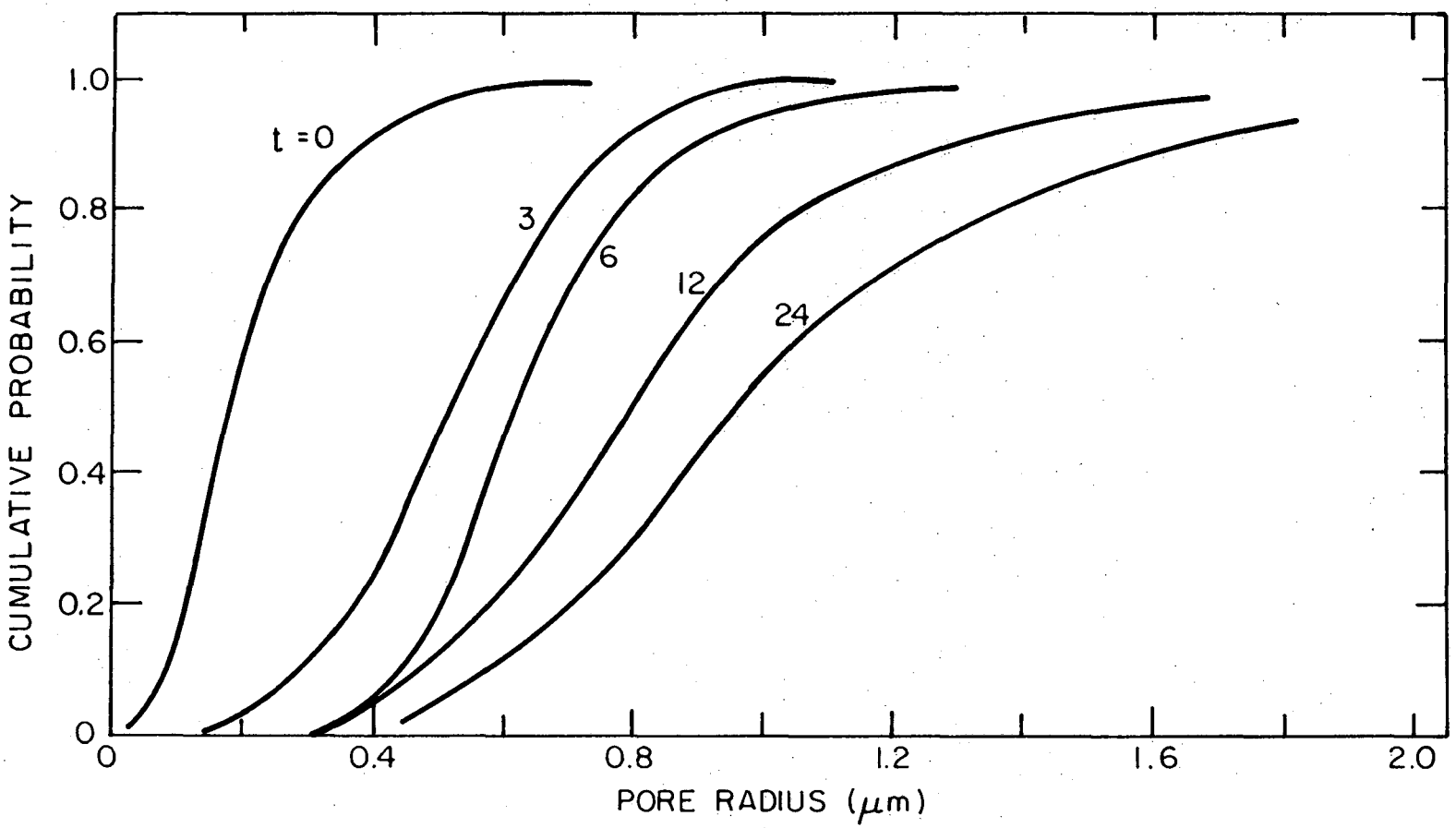


XBL826-5905

Fig. 6

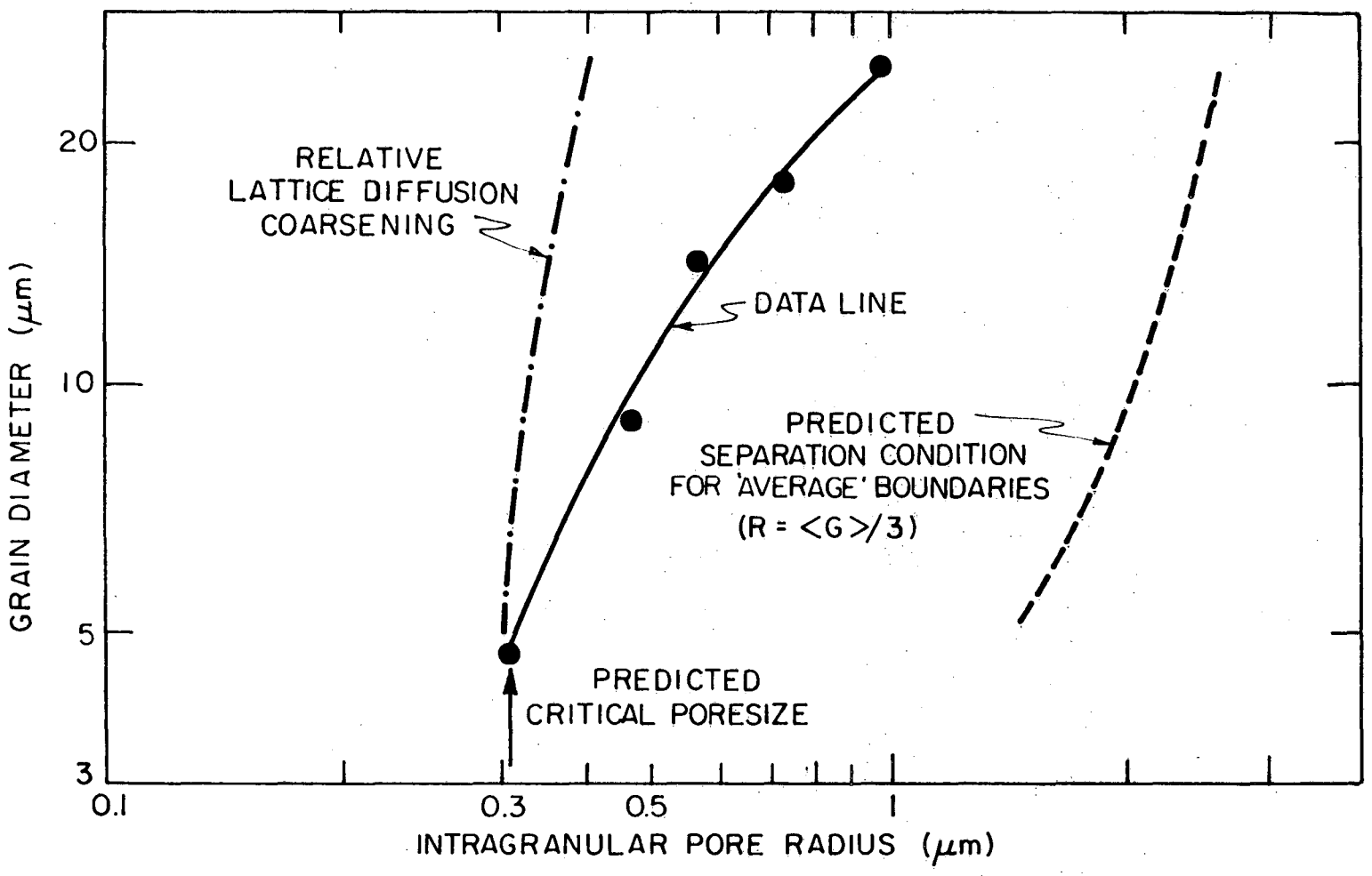


XBL 826-5906

Fig. 7

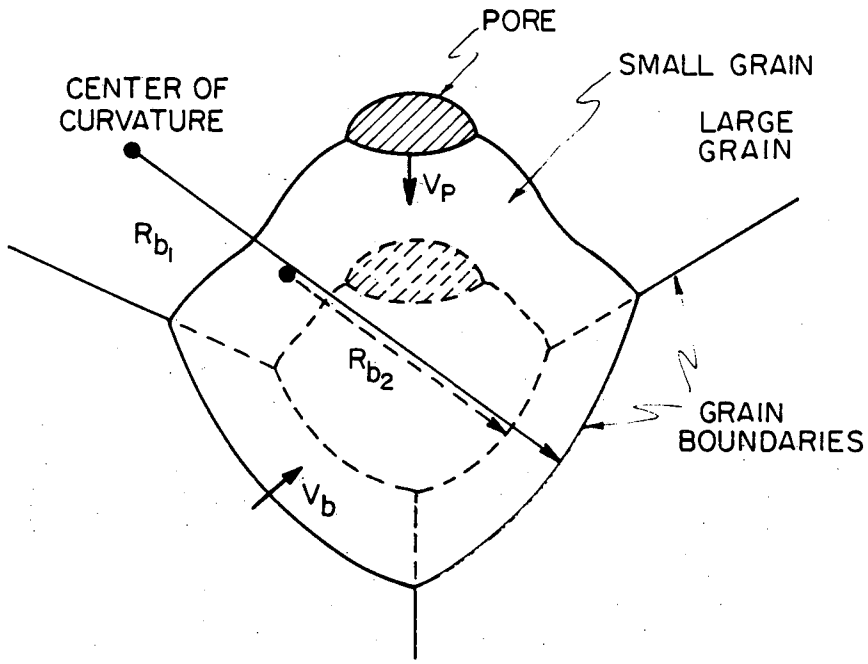


a) A DISAPPEARING THREE-SIDED GRAIN

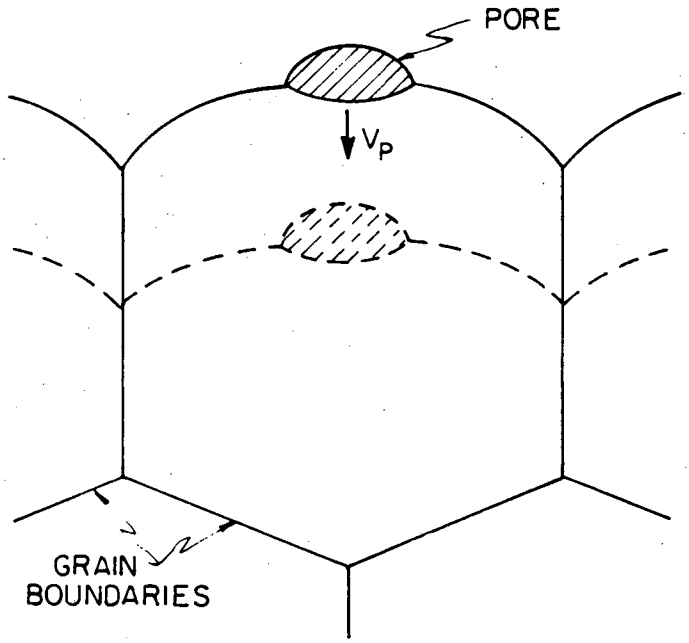


b) A GRAIN WITH UNIFORM DRIVING FORCE

XBL 826-5908

Fig. 8

This report was done with support from the Department of Energy. Any conclusions or opinions expressed in this report represent solely those of the author(s) and not necessarily those of The Regents of the University of California, the Lawrence Berkeley Laboratory or the Department of Energy.

Reference to a company or product name does not imply approval or recommendation of the product by the University of California or the U.S. Department of Energy to the exclusion of others that may be suitable.

*TECHNICAL INFORMATION DEPARTMENT*
*LAWRENCE BERKELEY LABORATORY*
*UNIVERSITY OF CALIFORNIA*
*BERKELEY, CALIFORNIA 94720*